energies

MDPI

Article

Resistance Separation of Polymer Electrolyte Membrane Fuel Cell by Polarization Curve and Electrochemical Impedance Spectroscopy

Jaehyeon Choi [1], Jaebong Sim [1], Hwanyeong Oh [2] and Kyoungdoug Min [1,*]

[1] Department of Mechanical and Aerospace Engineering, Seoul National University, 1 Gwanak-ro, Gwanak-Gu, Seoul 08826, Korea; wogus0922@naver.com (J.C.); sim6368@snu.ac.kr (J.S.)
[2] Fuel Cell Laboratory, Korea Institute of Energy Research, 152 Gajeong-ro, Yuseong-gu, Daejeon 34129, Korea; hyoh@kier.re.kr
* Correspondence: kdmin@snu.ac.kr; Tel.: +82-2-880-1661; Fax: +82-2-874-2001

Abstract: The separation of resistances during their measurement is important because it helps to identify contributors in polymer electrolyte membrane (PEM) fuel cell performance. The major methodologies for separating the resistances are electrochemical impedance spectroscopy (EIS) and polarization curves. In addition, an equivalent circuit was selected for EIS analysis. Although the equivalent circuit of PEM fuel cells has been extensively studied, less attention has been paid to the separation of resistances, including protonic resistance in the cathode catalyst layer (CCL). In this study, polarization curve and EIS analyses were conducted to separate resistances considering the charge transfer resistance, mass transport resistance, high frequency resistance, and protonic resistance in the CCL. A general solution was mathematically derived using the recursion formula. Consequently, resistances were separated and analyzed with respect to variations in relative humidity in the entire current density region. In the case of ohmic resistance, high frequency resistance was almost constant in the main operating load range (0.038–0.050 Ω cm^2), while protonic resistance in the CCL exhibited sensitivity (0.025–0.082 Ω cm^2) owing to oxygen diffusion and water content.

Keywords: resistance separation; overpotential; electrochemical impedance spectroscopy; polarization curve; protonic resistance

Citation: Choi, J.; Sim, J.; Oh, H.; Min, K. Resistance Separation of Polymer Electrolyte Membrane Fuel Cell by Polarization Curve and Electrochemical Impedance Spectroscopy. *Energies* **2021**, *14*, 1491. https://doi.org/10.3390/en14051491

Academic Editor: Alexandros Arsalis

Received: 17 February 2021
Accepted: 7 March 2021
Published: 9 March 2021

1. Introduction

Owing to increasing greenhouse gas emissions, global warming has become one of the biggest environmental problems of the 21st century. Approximately 17% of the CO_2 emissions originate from automotive internal combustion engines [1,2]. Accordingly, automobiles with polymer electrolyte membrane (PEM) fuel cells have gained attention, with the aim of achieving zero emissions and higher efficiency [3]. A PEM fuel cell converts the chemical energy of the reaction between H_2 and O_2 into electrical energy using pure water [3,4]. Hence, PEM fuel cell technologies have received significant research interest.

In this process, researchers require useful data on water management, ohmic losses, and the ionic conductivity of PEM to identify the research direction and operating conditions. The most frequently used methods are electrochemical impedance spectroscopy (EIS) and polarization curves. These have been generally used to procure information on resistance and current voltage, respectively [5,6].

As the technique for determining the equivalent circuit of the EIS technique is not proprietary [7], it has been the subject of study for a long time. It has been widely used in the case of lumped circuits, for which many types of equivalent circuits have been suggested [4,8–10]. However, the lumped circuit is not appropriate to describe the protonic resistance in the cathode catalyst layer (CCL), which represents a 45-degree straight line in the high-frequency region around the first arc [11–14]. It pushes away the first semi-

circle from the origin, and the distance from the x-intercept is proportional to the protonic resistance in the CCL. This distance is called the effective protonic resistance [15–20].

To describe this line, differential equations or the finite transmission-line model (TLM) are normally used [13,21,22]. Makharia et al. [13] reported the calculation of effective protonic resistance using differential equations and analyzed the results of the H_2/N_2 experiment. The sum of all the distributed proton transport resistances estimated from the TLM was approximately equal to three times the effective protonic resistance. However, in this process, the homogeneity of distributed elements in the TLM was assumed, and the experiments were carried out at low current densities.

Malevich et al. [23] studied the effect of inhomogeneity of elements in the TLM in the H_2/N_2 condition. The results showed that non-uniform distribution of proton conductivity and capacity affected the shape and angle of the 45-degree straight line around the high-frequency region. Thus, the effective protonic resistance in CCL was not one-third of the protonic resistance in CCL. Furthermore, Gerteisen [24] studied the impact of the inhomogeneity of charge transfer resistance in the H_2/air condition, which affected the charge transfer arc.

As the non-uniformity of charge transfer resistance affected the total resistance, Gaumont et al. [16] suggested a general solution that included a non-uniform distributed charge transfer resistance in the CCL. The general solution was derived using an equivalent circuit with current distribution throughout the thickness of the electrode. Although this work considered the variation in distributed charge transfer resistance, the equivalent circuit did not take into account the effects of mass transport resistance or diffusion.

Cruz-Manzo and Chen [1] suggested using the TLM together with the Bounded Warburg to reflect the diffusion effect in the CCL in the entire current density region [25]. The authors evaluated the differential equations and suggested an electrical equivalent circuit but did not attempt an estimation using a recursion formula. To solve the differential equations, it was assumed that the protonic resistance in CCL ought to be much smaller than the charge transfer resistance.

While EIS analysis provides detailed information on each component of resistance, the polarization curve is also commonly used to investigate the general quantification of performance [5]. As each of these two experiments provides different sets of information, several researchers have used both [4,26,27]. Tang et al. [28] compared the cell voltage drop owing to each resistance component using EIS and polarization curves. To compare the two experimental results, each resistance component was evaluated via EIS, following which the voltage drop was estimated and compared with that obtained from the polarization curve. Consequently, the authors suggested a methodology to compare the results of EIS with those of the polarization curve; however, the protonic resistance in the CCL was not considered.

Several works have been conducted using EIS analysis and polarization curves. However, owing to deficiencies in the methodologies' ability to separate the estimation of each resistance, the estimation of each component of resistance (charge transfer resistance, high frequency resistance (*HFR*), mass transport resistance, and effective protonic resistance in the CCL) has not been sufficiently carried out. In the present study, these four types of resistances, especially including effective protonic resistance in the CCL, were considered to derive a general solution of the impedance model. From this general solution, a new method was proposed to evaluate the total resistance.

When the distributed elements in the TLM were homogeneous and the distributed protonic resistance in the CCL was less than the summation of the distributed charge transfer resistance and mass transport resistance, each resistance component was evaluated using EIS alone. In other cases, the correlation between EIS analysis and the polarization curve was used. Thus, the total resistance of a PEM fuel cell was quantitatively determined. This was conducted by varying current densities and conditions of relative humidity (RH), EDIT, and the resultant variations in resistance were analyzed.

2. Experiment

2.1. Experimental Setup

The measurements for EIS analysis and polarization curve were carried out under the experimental conditions listed in Table 1. A commercialized product called GORE^{TM} PRIMEA$^{®}$ 5730 was used to improve the validity and reproducibility of the experimental results. Before measuring the EIS data, the voltage and current density were measured to plot the polarization curve, because the measurements in both cases were carried out under identical conditions. For these experiments, an FC impedance meter (KFM 2150 and PLZ-4W) was used. To satisfy EIS assumptions such as linearity and stability, the potential amplitude was maintained at lower than 10 mV. For the sinusoidal alternating current (AC) signal, the frequency range analyzed was 20 kHz to 900 mHz. However, to ensure the existence of another semi-circle appearing at low frequency, the end frequency was 10 mHz in the high current density region. The high frequency resistance was measured at 20 kHz resistance. The electronic bulk resistance and contact resistance components of the *HFR* were measured using an ex situ direct current (DC) experiment with a PEM fuel cell, except for the membrane electrode assembly (MEA). The temperature and pressure were maintained at 65 °C and ambient pressure, respectively.

Table 1. Operating conditions for measuring the EIS and polarization curve.

Parameter	Condition
Test mode	Galvanostatic technique
Frequency	20 kHz to 900 mHz
Swing width of AC current	within a voltage amplitude of less than 10 mV
Current density	0.1–2.4 A/cm^2
Mass flow	Anode: 0.400 ln/min (SR * > 20) Cathode: 2.00 ln/min (SR * > 40)
Reactant gas	H_2/air H_2/Heliox (21% O_2 with the balanced made of He)
Inlet gas RH **	50, 80, 100% (anode/cathode)
Cell temperature	65 °C
Outlet pressure	Ambient pressure

* Stoichiometric ratio, ** relative humidity.

Table 2 lists the materials of the fuel cell used in this work. As shown in Figure 1, the 1 cm^2 active area near the outlet of the 25 cm^2 flow channel was assembled using a gasket and gas diffusion layer (GDL), which provides in-plane uniformity to resistance, current distribution, and reactant gas. Thus, a single cell was used to control the operating conditions as well.

Table 2. Specifications of the unit cell.

Component	Condition
Flow Channel	Parallel channels (anode/cathode) 1/0.815 mm width (channel/rib) 0.4/0.6 mm depth (anode/cathode)
GDL-MPL	JNT30-A6H (Thickness 325 ± 5 μm)
MEA †	GORE^{TM} PRIMEA$^{®}$ 5730 ‡

† Membrane electrode assembly, ‡ catalyst-coated membrane.

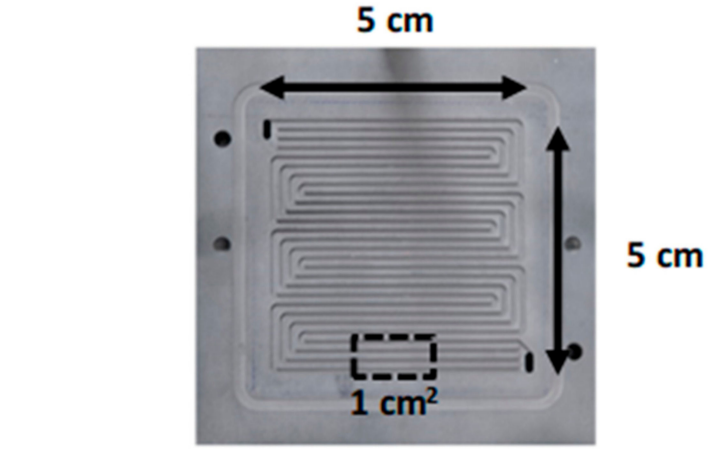

(**a**)

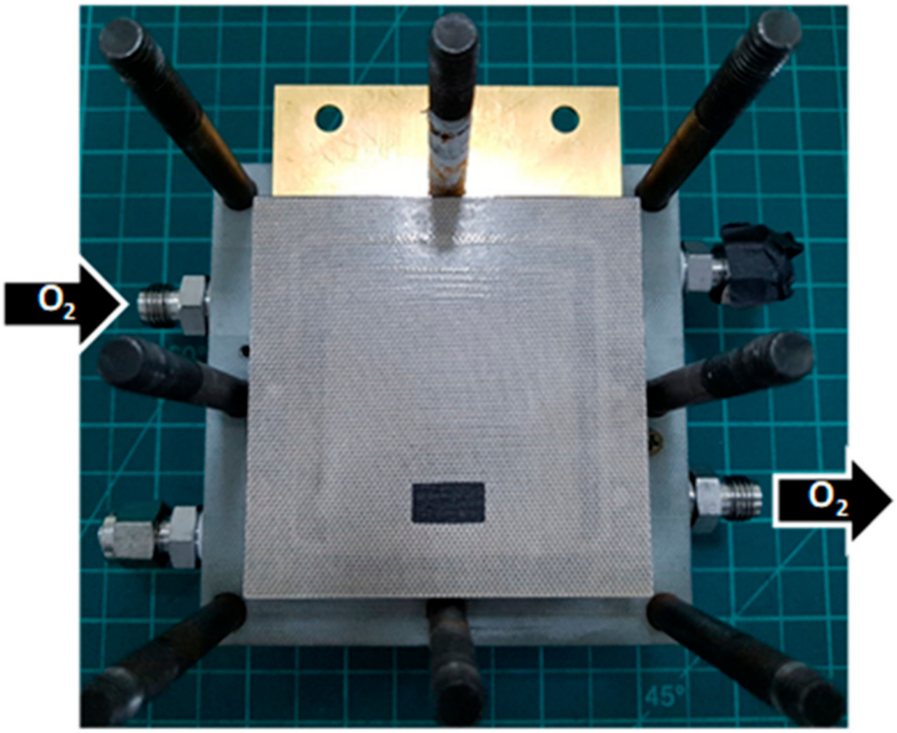

(**b**)

Figure 1. Setup of the active area. (**a**) Flow channel. (**b**) Assembly of end plate, flow channel, gasket, and gas diffusion layer (GDL).

2.2. Experimental Conditions and Assumptions

Unlike in other fuel cell experiments, the use of EIS analysis and polarization curves in the present work requires high stoichiometry ratios (SR) and a small active area for the following assumptions related to the impedance model.

- The SR has to be kept high to minimize reactant depletion along the channels. This setup also creates a condition of high diffusion through the CCL.
- The active area of the fuel cell needs to be small to have a uniform pressure and velocity.

This study used the current distribution equation, Equation (7), suggested by Eikerling and Kornyshev [29], which assumed fast oxygen diffusion, and hence a high SR condition was applied. The RH of the inlet gas was varied in the range from 50% to 100% to investigate

its effect on resistance. The current was varied in the range from 0.1 to 2.4 A/cm^2 in increments of 0.1 A/cm^2 to compare the EIS and polarization curve results.

3. Impedance Model

3.1. Electrical Equivalent Circuit

A reasonable selection of an electrical equivalent circuit is an essential step before the analysis of the experimental data. The rate of hydrogen oxidation is greater than that of oxygen reduction reaction, and hence, the anode resistance can be neglected [17,30–32]. In addition, the ohmic resistance caused by the electron flow in the CCL can be neglected because the electronic resistance in the CCL is smaller than the ionic resistance. Moreover, the anode resistance and the electronic resistance in the CCL were not critical, as shown in our experimental results, and were therefore neglected as in previous studies [13,16,17,30–32]. Unlike other equivalent circuits, the bounded constant phase element (BCPE) in the TLM was required to represent the mass transport effect in the CCL. Thus, the equivalent circuit suggested by Cruz-Manzo and Chen [1] was used in the present work. To improve the fitting results, the Bounded Warburg was replaced with the BCPE, and the element of the inductor was eliminated, as shown in Figure 2.

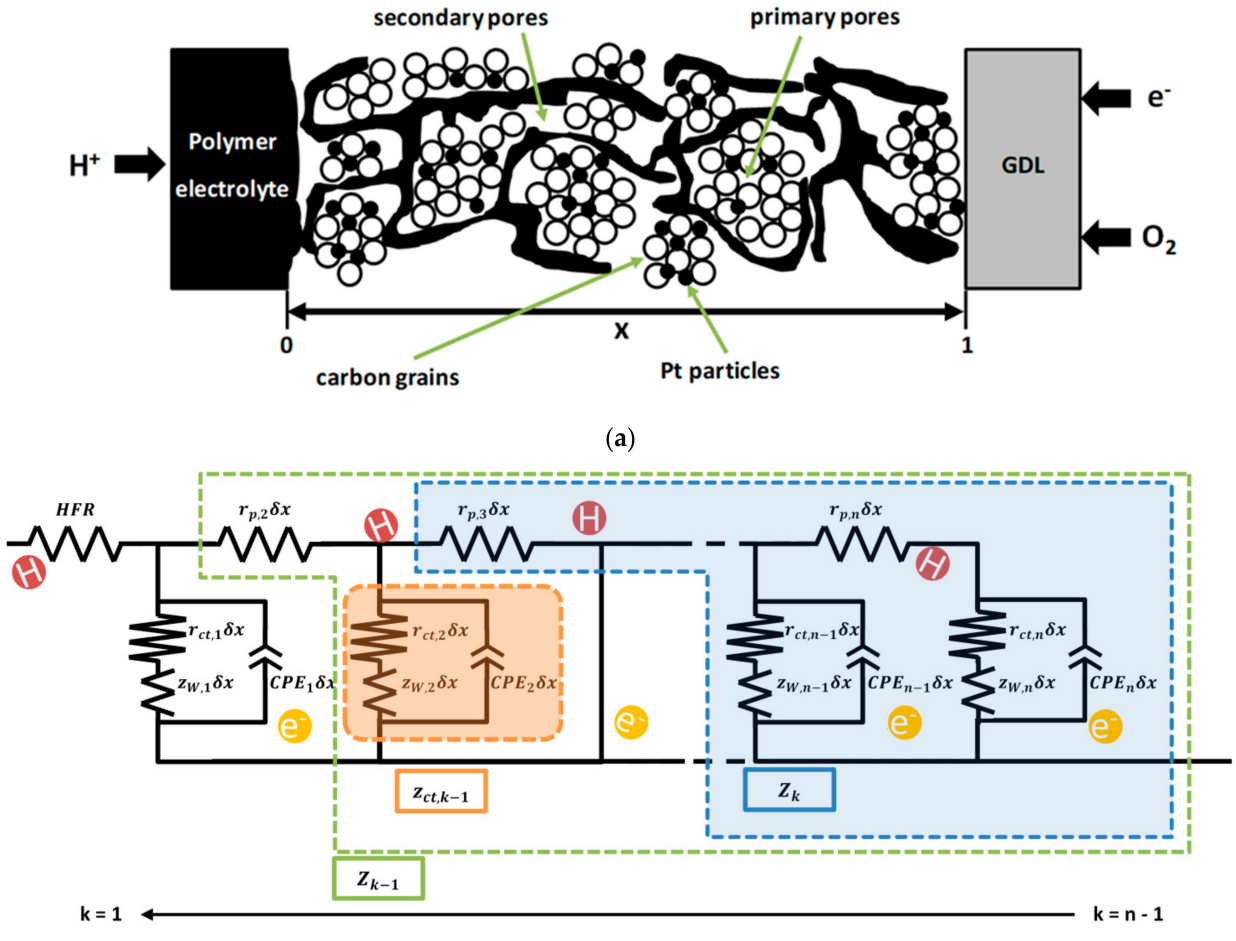

Figure 2. (**a**) A schematic of the catalyst layer (CCL). $x$represents the non-dimensional thickness of the CCL from the CCL/GDL interface ($x = 1$) to the polymer electrolyte membrane (PEM)/CCL interface ($x = 0$). (**b**) Electrical equivalent circuit of a PEM fuel cell represented by a transmission-line model (TLM) [1].

The HFR includes the electronic bulk resistance, contact resistance, and resistance due to proton conduction in the membrane. The TLM shown in Figure 2 represents the catalyst

layer, which includes the distributed protonic resistance in the CCL (r_p), distributed charge transfer resistance (r_{ct}), distributed BCPE (z_W), and constant phase element (CPE) for the double-layer capacitance. Here, n is the total number of iterations, and k is the iteration number of the node in the interval ($1 \leq k \leq n-1$). Referring to a previous work, n is 1000 [16].

3.2. General Solution

To represent the Nyquist plot using the TLM, the general solution was used with the recursion formula [16]. The CCL section of the Nyquist plot can be evaluated iteratively using the recursion formula from the CCL/GDL interface to the PEM/CCL interface as follows.

$$\begin{cases} Z_n = z_{ct,n} + r_{p,n}\delta x \\ Z_k = \left(\frac{1}{Z_{k+1}} + \frac{1}{z_{ct,k}}\right)^{-1} + r_{p,k}\delta x \,,\, r_{p,1} = 0 \end{cases} \quad (1)$$

with

$$\begin{cases} \delta x = \frac{l}{n} \\ CPE_k = q_{C,k}(iw)^{P_{C,k}} \\ z_{ct,\,k} = \left[\left\{r_{ct,k}\delta x + z_{W,k}\delta x\right\}^{-1} + CPE_k\delta x\right]^{-1} \\ z_{W,k} = \frac{tanh\left(r_{mass,k}\delta x^2\ q_{B,k}(iw)^{P_{B,k}}\right)}{q_{B,k}(iw)^{P_{B,k}}\ \delta x^2} \end{cases} \quad (2)$$

where l, x, r_{mass}, q_C, P_C, i, w, q_B and P_B are the thickness of the CCL, the non-dimensional distance along the CCL ($0 \leq x \leq 1$), the distributed mass transport resistance, the distributed parameter related to CPE, the CPE exponent, the imaginary component in the impedance, the frequency, the distributed parameter related to BCPE, and the BCPE exponent, respectively.

To apply the inhomogeneity of r_{ct}, r_{ct} is calculated as follows [16,29]

$$r_{ct,k} = \frac{b}{j(x)}\frac{1}{\delta x^2} \quad (3)$$

with

$$j(x) = \frac{\sqrt{2i^*\sigma b}}{l} \cdot \exp\left(\frac{\eta_1}{2b}\right) \cdot tan\left(\sqrt{\frac{i^*}{2\sigma b}}(1-x)\exp\left(\frac{\eta_1}{2b}\right)\right) \quad (4)$$

where b is the Tafel slope, σ is the proton conductivity, i^* is the exchange current density, and η_1 is the overpotential at the PEM/CCL interface. This equation can be used under the assumption of rapid oxygen diffusion. A single parameter, Equation (5), is used to check this assumption in this experimental condition. The detailed derivation of the Equations (4) and (5) is given in Ref. [29].

$$g = \frac{4FPD^{eff}}{RTl}\frac{1}{\sigma b} \quad (5)$$

It was estimated to be in the range 14–250 based on the experimental results. D^{eff} and σ can be estimated from BCPE. Thus, Equation (4) can be used in this study because $g \gg 1$.

3.3. Resistance Separation Using EIS

The general solution with the recursion formula was derived in the last section. However, the distributed resistance from the general solution is not convenient to separate the total resistance (R_{total}). As the experimental conditions, two techniques were suggested. First, when the distributed elements are homogeneous and $r_p/(r_{ct}+r_{mass}) \ll 1$, resistance separation is conducted using EIS. On the other hand, not only EIS but also the polarization curve are conducted when the distributed elements are not homogeneous or $r_p/(r_{ct}+r_{mass})$ is not much smaller than 1. In this section, the first case was investigated. The second case was investigated in Section 3.5. To divide R_{total} into the effective protonic resistance in the

CCL (R_p^{eff}), charge transfer resistance (R_{ct}), and mass transport resistance (R_{mass}) using the distributed elements, three assumptions were applied.

- The distributed elements in the CCL are homogeneous [33].
- $r_p/(r_{ct}+r_{mass}) \ll 1$.
- As previously mentioned, the anode resistance and the electronic resistance in the CCL are neglected.

To check the validity of the first assumption, a Nyquist plot was plotted using Equation (1) with homogeneous distributed elements, and then it was compared to the EIS experimental results.

R_{total} is the most important information obtained in this study. A point at the intersection of the real axis at a low frequency is extracted from Equation (1) [34].

$$\begin{aligned} R_{total} &= \lim_{w\to 0}(HFR + Z_1) \\ &= HFR + \frac{r_{ct}\delta x + r_{mass}\delta x}{A_{n-1}+1} + r_p\delta x \end{aligned} \tag{6}$$

with

$$A_{n-k} = \frac{(A_{n-k-1}+1)(r_{ct}+r_{mass})}{(r_{ct}+r_{mass})+(A_{n-k-1}+1)r_p}, \quad A_0 = 0 \tag{7}$$

Then, a general term can be derived as follows. From Equation (7),

$$A_{n-k} = A_{n-k-1} + 1 - \frac{r_p}{r_{ct}+r_{mass}} \cdot \frac{(A_{n-k-1}+1)^2}{1+(A_{n-k-1}+1)\cdot\frac{r_p}{r_{ct}+r_{mass}}} \tag{8}$$

Based on the second assumption,

$$A_{n-k} \approx A_{n-k-1} + 1 - \frac{r_p}{r_{ct}+r_{mass}} \frac{(A_{n-k-1}+1)^2}{1} \tag{9}$$

When k is large, Equation (8) can be approximated to a simple form as shown below; because both $r_p/(r_{ct}+r_{mass})$ and $(A_{n-k-1}+1)^2$ are small.

$$A_{n-k} \approx A_{n-k-1} + 1 \tag{10}$$

$$A_{n-k} \approx n-k \tag{11}$$

Therefore, the right-hand side of Equation (9) can be simplified as Equation (12) using Equation (11). At this point, the error caused by Equation (11) is only acceptable when k is large. Therefore, the error in the third term on the right-hand side can be approximated using Equation (11) due to $r_p/(r_{ct}+r_{mass})$. However, Equation (11) is not applicable to the first term on the right-hand side, because the error in this term is not negligible without multiplication by $r_p/(r_{ct}+r_{mass})$.

$$A_{n-k} \approx A_{n-k-1} + 1 - \frac{r_p}{r_{ct}+r_{mass}} \cdot (n-k)^2 \tag{12}$$

Finally, the general term of the recursion formula is derived from Equation (12).

$$A_{n-k} \approx n-k - \frac{r_p}{r_{ct}+r_{mass}} \frac{(n-k)(n-k+1)(2n-2k+1)}{6} \tag{13}$$

To check the derivation of this equation, Equations (7), (11), and (13) are plotted as shown in Figure 3. When k is large, three lines are well matched. However, Equation (11) is not well matched when k is small.

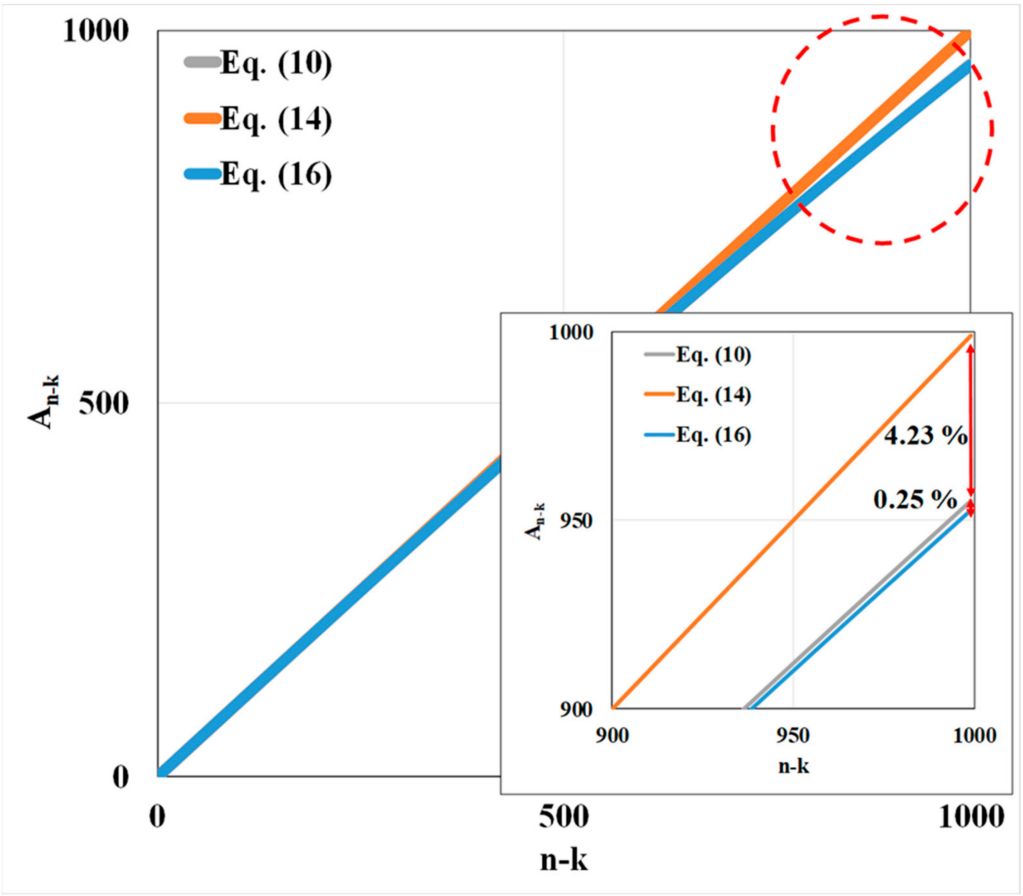

Figure 3. Equation (7) is simplified. Equation (11) can be used only if the k is large. On the other hand, the error in Equation (13) is less than 0.25% at 0.1 A/cm^2, so this equation can be used regardless of the k.

The general term can be derived by substituting Equation (13) into Equation (6).

$$R_{total} = HFR \quad + \frac{\frac{r_{ct}\delta x + r_{mass}\delta x}{n-1-\frac{r_p}{r_{ct}+r_{mass}}\frac{(n-1)(n)(2n-1)}{6}+1}}{+r_p\delta x} \tag{14}$$

When the first assumption is valid [33], Equation (14) can be rearranged as follows [17,34].

$$\begin{aligned} R_{total} &= R_{ct} + R_{ohmic} + R_{mass} \\ &= R_{ct} + HFR + R_P^{eff} + R_{mass} \end{aligned} \tag{15}$$

with

$$R_P^{eff} = \frac{\frac{r_p\delta x(n-1)(2n-1)}{6n}}{1-\frac{r_p}{r_{ct}+r_{mass}}\frac{(n-1)(2n-1)}{6}} + r_p\delta x \tag{16}$$

$$R_{ct} = \frac{r_{ct}\delta x}{n} \tag{17}$$

$$R_{mass} = \frac{r_{mass}\delta x}{n} \tag{18}$$

where R_{ohmic} is the ohmic resistance of the summation of HFR and R_P^{eff}.

3.4. Validation of Recursion Formula

In this section, the general solution (Equations (1)–(4)) and the general term (obtained by substituting Equation (13) into Equation (6)) were validated using the solution suggested by Cruz-Manzo and Chen [1] and our experimental results.

Cruz-Manzo and Chen [1] suggested not only an equivalent circuit but also a solution of differential equations for the impedance model depicted in Figure 2. This solution, the validation model, was used to validate the general solution. After disregarding the inductance term and replacing the Bounded Warburg with the BCPE, the final total impedance equation can be written as follows:

$$Z_{total} = HFR + \frac{[R_{ct} + Z_W]\gamma_1 \coth(\gamma_1(1-x))}{1 + Q_C(iw)^{P_C}[R_{ct} + Z_W]} \tag{19}$$

with $\gamma_1 = \sqrt{R_p\left[\frac{1}{R_{ct}+Z_W} + Q_C(iw)^{P_C}\right]}$

$$Z_W = \frac{tanh\left(R_{mass}Q_B(iw)^{P_B}\right)}{Q_B(iw)^{P_B}} \tag{20}$$

where R_p is protonic resistance in the CCL, Z_W is the BCPE, Q_C is the parameter related to the CPE, and Q_B is the parameter related to the BCPE. To derive Equation (19), it was assumed that the element in the CCL was homogeneous. Furthermore, to satisfy the homogeneity of r_{ct}, Equation (21) should be valid [1].

$$\frac{R_p}{R_{ct}} \ll 1 \tag{21}$$

Figure 4 shows the fitting results of the general solution and validation model. Both models fitted well with the experimental results at RH 80% and 100%, regardless of the current densities. However, the general solution did not fit well with the validation model at RH 50%. The results can be explained based on the assumption of the homogeneity of r_{ct}. The value of $r_p/(r_{ct} + r_{mass})$ was much smaller than 1 ($3.5 \times 10^{-7} > r_p/(r_{ct} + r_{mass}) > 7.6 \times 10^{-8}$) regardless of the RH conditions. Thus, it was inferred that the mismatch at RH 50% was caused by the inhomogeneity of r_{ct} in the TLM. As a result, the homogeneous assumption of r_{ct} can be valid at RH 80% and 100%.

On the other hand, as the straight line in our experimental data was maintained at 45 degrees, it seems that the impacts of the inhomogeneity of the double layer capacity and protonic conductivity might not be significant, similar to what was found in previous research [24].

Furthermore, the general term was validated using R_{total}, which was evaluated from the experimental data. By comparing the R_{total} values obtained from the general term, Equation (18), and the general solution, Equation (9), the error of the general term was less than 1% at RH 100%, regardless of the current density. However, the error increased as RH decreased. The maximum error at RH 80% was around 1.5%. Therefore, the error caused by the assumption that $r_p/(r_{ct} + r_{mass}) \ll 1$ was not significant at RH 80%, 100%. Consequently, resistance separation can be carried out using Equations (15)–(18) when the TLM is homogeneous and RH is greater than 80%.

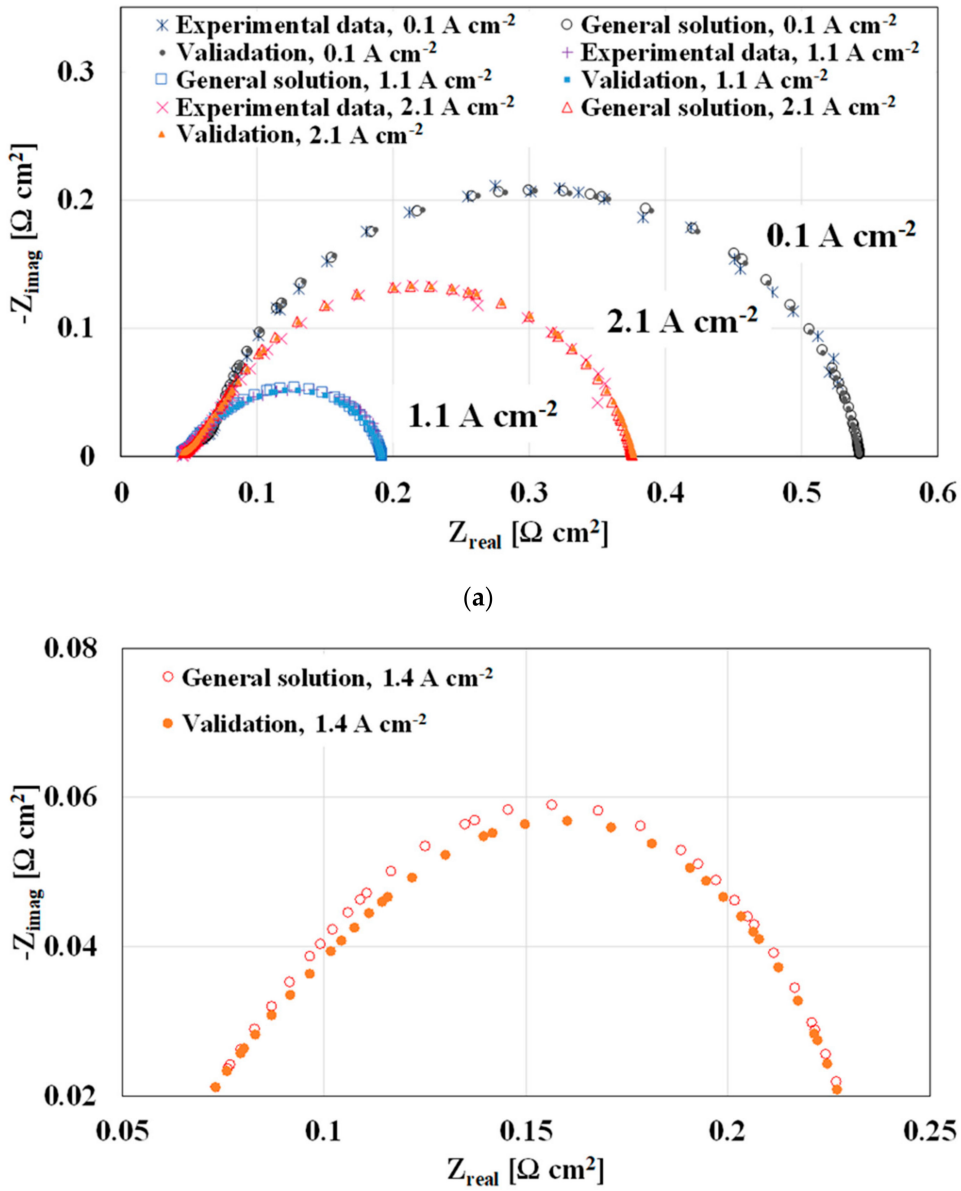

Figure 4. (**a**) Nyquist plots are plotted at relative humidity (RH) 100%, (**b**) RH 50% under H_2/air condition. Open symbols represent general solution and closed symbols represent validation model. Cross symbols represent experimental data.

In addition, $R_P^{eff} \approx R_p/3$ can be derived. From Equation (19), because $n \gg 1$ (in this study, n is 1000), $n \approx n-1 \approx \frac{2n-1}{2}$.

$$R_P^{eff} \approx \frac{\frac{nr_p\delta x}{3}}{1-\frac{r_p}{r_{ct}+r_{mass}}\frac{n^2}{3}} + r_p\delta x \tag{22}$$

If $r_p\delta x^2/(r_{ct}+r_{mass}) \approx 0$ and $r_p\delta x \ll \frac{nr_p\delta x}{3}$,

$$\begin{aligned} R_P^{eff} &\approx \frac{r_p\delta x\left(1-\frac{r_p}{r_{ct}+r_{mass}}\frac{n^2}{3}\right)+\frac{nr_p\delta x}{3}}{1-\frac{r_p}{r_{ct}+r_{mass}}\frac{n^2}{3}} \\ &\approx \frac{nr_p\delta x}{3} \\ &\approx \frac{R_p}{3} \end{aligned} \tag{23}$$

3.5. Resistance Separation Using the Correlation between EIS and Polarization Curve

In the last two sections, resistance separation using EIS was investigated, when the distributed elements are homogeneous and approximation of $r_p/(r_{ct}+r_{mass})$ is valid. However, in some cases, the approximation of $r_p/(r_{ct}+r_{mass})$ or the assumption onf the homogeneity of r_{ct} may not be valid. The experimental results of middle or high current densities under the H_2/Heliox condition showed that the assumption $r_p/(r_{ct}+r_{mass}) \ll 1$ was not correct, because r_{mass} was low. This section suggests another methodology for a use under this condition, because the resistance separation using Equations (15)–(18) is no longer applicable. For this reason, the correlation between EIS and polarization curve is applied to separate the resistance. Naturally, resistance separation can be carried out using a polarization curve alone [28]; however, the additional analysis of the EIS results is helpful to consolidate the validity of the resistance separation.

The polarization curves, shown in Figure 5, are expressed using a semi-empirical equation [35]:

$$E = E_0 - b\ln\left(I{\cdot}10^3\right) - IR_{ohmic} - m_{mass}\exp(n_{mass}I) \tag{24}$$

where E is the cell voltage, E_0 is the open-circuit voltage (OCV), I is the current density, m_{mass} is the mass transport coefficient, and n_{mass} is the simulation parameter for the polarization curve fitting. For resistance separation based on Equation (24) [17],

$$\begin{aligned} R_{total} &= R_{ct} + R_{ohmic} + R_{mass} \\ &= \tfrac{dE}{dI} \\ &= \tfrac{b}{I} + R_{ohmic} + m_{mass}n_{mass}\exp(n_{mass}I) \\ &= \tfrac{b}{I} + HFR + R_P^{eff} + m_{mass}n_{mass}\exp(n_{mass}I) \end{aligned} \tag{25}$$

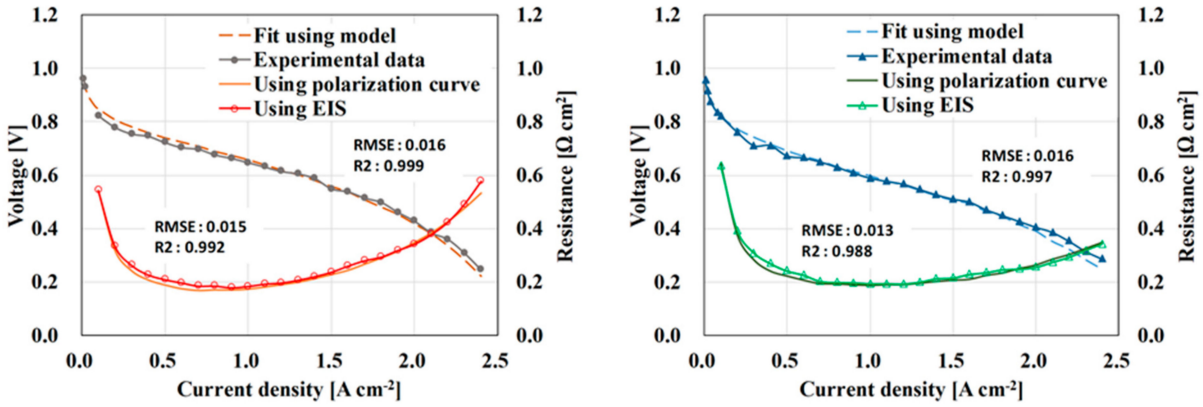

Figure 5. Polarization curves and total resistances at (**a**) RH 100%, (**b**) RH 80% under H_2/air experiments. The experimental data of polarization curves were fitted using semi-empirical model. The total resistances using electrochemical impedance spectroscopy (EIS) were matched with the total resistances using polarization curves.

HFR is evaluated via EIS regardless of the current density region. Meanwhile, R_{ct} and R_{mass} are estimated using EIS analysis and the polarization curve. In general, in the region of low current density, the approximation of $r_p/(r_{ct}+r_{mass})$ and the assumption of the homogeneity of r_{ct} can be used [13,16]. Thus, the unknown parameters in Equation (24), namely E_0, b, m_{mass}, and n_{mass}, are determined using the experimental data of the EIS at low current densities. By Equation (25), the values of R_{ct} and R_{mass} can be estimated when $r_p/(r_{ct}+r_{mass})$ is large or r_{ct} is not homogeneous. Finally, R_P^{eff} can be evaluated using Equation (25), because R_{total} is found by the EIS and polarization curve. Consequently, although $r_p/(r_{ct}+r_{mass})$ is not small and r_{ct} is not homogeneous, the resistance can be separated using Equation (25) and the fitting results of the other current density regions.

Summary of solutions explain on Table 3.

Table 3. Summary of solutions.

	R_p and R_{mass}	Inhomogeneity of Elements	Resistance Separation
Solution suggested by Cruz-Manzo and Chen	Considered	Not considered	Facile
General solution	Considered	Considered	Arduousness
Approximated solution with homogeneous elements	Considered	Not considered	Facile
Approximated solution with inhomogeneous elements	Considered	Considered	Facile

4. Results and Discussion

4.1. Comparison between EIS and Polarization Curve

As shown in Figure 5, the polarization curves obtained from our experimental results fitted well with fitting Equation (24). Differentiating the fitting equation with respect to I provided the information on resistance, as mentioned in Section 3. These results were also fitted well with the experimental data of the EIS, as shown in Figure 6 ($R^2 > 0.995$ and RMSE < 0.01). As reported in previous studies [36,37], R_{ct} increased as RH decreased. The R_{mass} at RH 100% was greater than that at RH 80% in the high current density region; however, these results were not maintained in the low current density region [4,38,39]. Furthermore, from the results of the R_{ohmic} at low current densities, as shown in Figure 7, the generated water in the CCL also affected R_{ct} and R_{mass} owing to the change in the ORR pathways, proton activity, and catalyst surface condition [36].

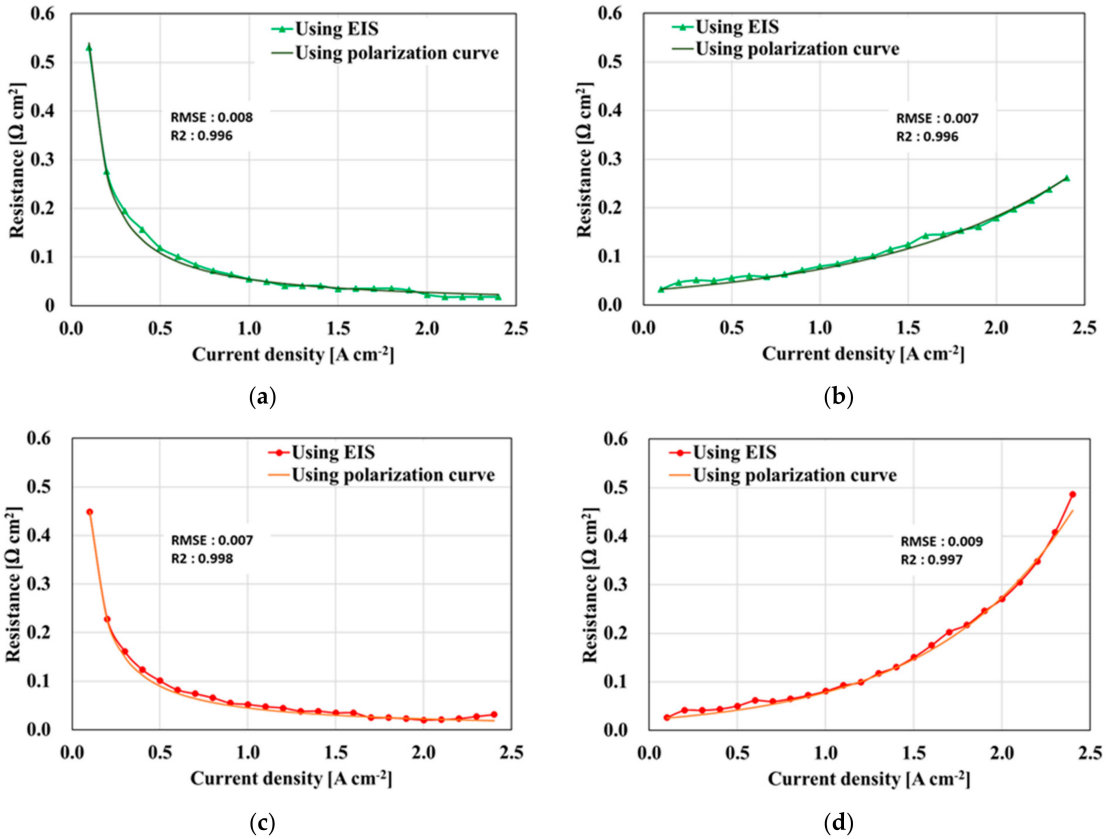

Figure 6. Results of the resistance separation under H_2/air. (**a**) Charge transfer resistance at RH 80%. (**b**) Mass transport resistance at RH 80%. (**c**) Charge transfer resistance at RH 100%. (**d**) Mass transport resistance at RH 100%.

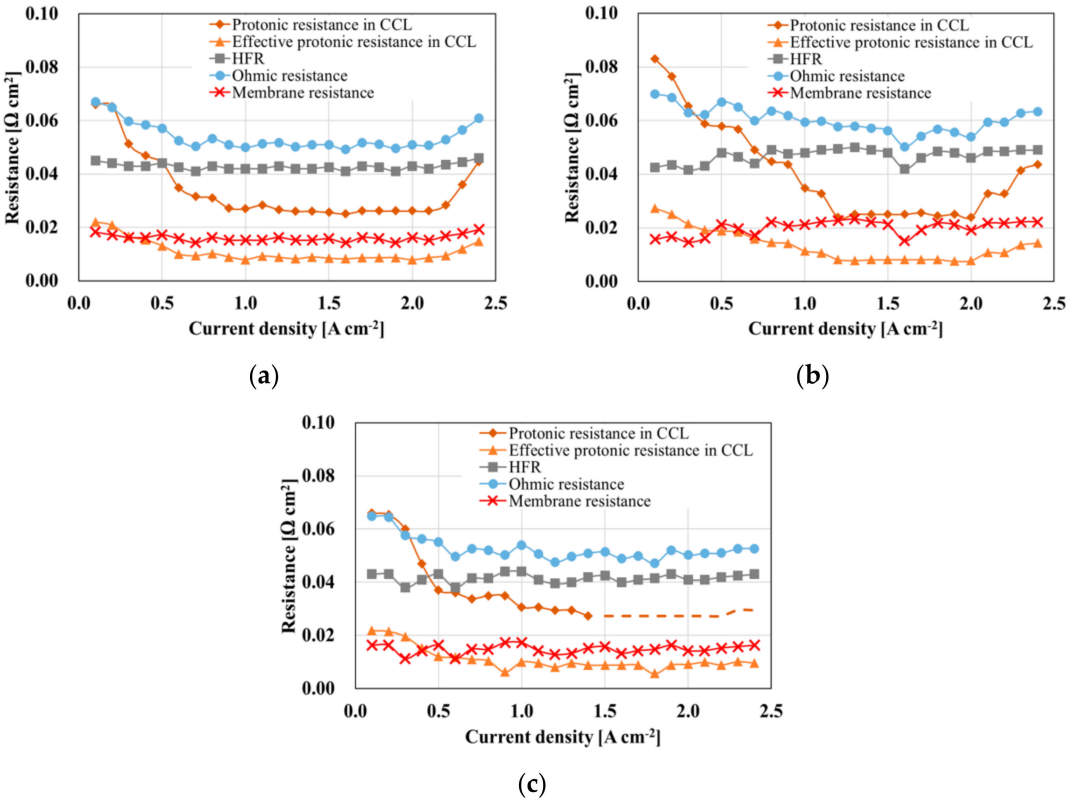

Figure 7. Separation of the ohmic resistance at (**a**) RH 100% under H_2/air, (**b**) RH 80% under H_2/air, and (**c**) RH 100% under H_2/Heliox. The rhombus symbol is the R_p, triangle symbol is the R_P^{eff}, the square symbol is HFR, and the circle symbol is ohmic resistance. At the dotted line, the fitting of the EIS was not well fitted, so protonic resistance in CCL cannot be evaluated. In this region, resistance separation was conducted using the correlation between EIS and the polarization curve.

4.2. Comparison of the Effective Protonic Resistance in CCL and Membrane Resistance with RH and Current Density

As the electronic bulk and contact resistances in HFR remained constant with variations in RH and current density, it was inferred that the change in HFR was caused by the variation in membrane resistance. As shown in Figure 7a,b, R_{ohmic} was divided into HFR and R_P^{eff} using EIS analysis and polarization curve in the experiment in H_2/air. It is already well known that the protonic resistance in Nafion is mostly determined by the water content [40,41]. In addition, the water content is closely related to RH and current density. As RH and current density were varied, R_{ohmic} notably changed owing to R_P^{eff}, but HFR was affected only a little. In other words, compared with HFR, R_P^{eff} was more sensitive to the operating current density and RH condition because of the water content. Furthermore, the change in R_P^{eff} was also highly related to the mean distance of ionic transport. The reaction rate and proton flow increased with current density. This means that in the low current density region, the effect of the increase in water content owing to the reaction was more critical than that of the increase in proton flow. This effect was equilibrated around the middle current density region, and thus, R_P^{eff} became constant. Thereafter, R_P^{eff} increased again owing to the high proton flow in the high current density region.

Additionally, the lowest levels of R_P^{eff} were almost the same at identical current densities (1.3–1.8 A cm^{-2}) regardless of the RH condition. It appeared that the CCL was fully hydrated at these operating conditions, although the RH was 80%.

The summation of the electronic bulk resistance and contact resistance in HFR was 0.026 Ωcm^2. This is a reasonable value when compared with that obtained in a previous study [13]. Based on this measurement, the protonic resistance in the membrane can be

evaluated. Therefore, the protonic resistance in the membrane was greater than in the CCL in the middle and high current density regions shown in Figure 7a,b. One of the reasons for this is the thickness of the MEA, which was measured using scanning electron microscope (SEM) images. The thickness of the membrane was 15.00 ± 1.5 μm, and that of the CCL was 10.91 ± 1.5 μm. Based on Ohm's law, the resistance in the membrane should be greater than that in the CCL, similar to the trend observed in the experimental results. The second reason pertains to the diffusion effect and distance of proton flow. The protons migrated through the electrolyte, but the distance of movement changed with the diffusion of the reactant gas and proton conductivity. In the membrane, the protons migrated from the anode to the cathode; thus, the distance of proton movement was greater than or equal to the thickness of the membrane. However, in the CCL, the distance of proton movement was less than or equal to the thickness of the CCL because O_2 also migrated to the triple phase boundary. Hence, the effective diffusion coefficient (D^{eff}) affected the R_P^{eff}. To confirm this effect, a H_2/Heliox experiment was conducted to vary D^{eff}, as shown in Figure 7c. As a result, R_P^{eff} decreased at high current densities, because the distance of proton flow in the CCL decreased. In other words, several reactant points were moved to the nearby membrane.

$R_P^{eff} \approx R_p/3$ is a well-known equation used to evaluate R_P^{eff}. This equation can be derived from Equation (16), and the error can be estimated as well. To derive the equation, $r_p/(r_{ct} + r_{mass})$ was assumed to be very small ($r_p/(r_{ct} + r_{mass}) \approx 0$). This was stricter than the assumptions with Equation (8) to (13). Therefore, the error owing to the assumptions with Equation (8) to (13) was less than 1.5%, but the error due to Equation (23) was more than 5.8% at RH 80% and 7.1% at RH 100%. In this context, R_P^{eff} was roughly $R_p/3$, but this assumption was not validated in the main operating load range, as shown in Figure 7.

5. Conclusions

The separation of resistances was investigated using EIS analysis and polarization curves. To analyze the EIS, a general solution based on a recursion formula was derived and validated. The solution was simplified using three assumptions, and thus, R_{total} was divided into R_{ct}, HFR, R_P^{eff}, and R_{mass}. When the approximation of $r_p/(r_{ct} + r_{mass})$ or the assumption of the homogeneity of r_{ct} was not valid, the resistance separation was carried out using both EIS analysis and polarization curves. The HFR was estimated from the EIS. The R_{ct} and R_{mass} values were estimated using a polarization curve with the semi-empirical equation. In this case, the equation was identified by fitting the EIS data in the other current density regions that satisfied the assumptions. Therefore, R_P^{eff} was calculated using other resistances obtained from the polarization curve and EIS.

The experimental results of R_{ohmic} suggested that HFR and R_P^{eff} were sensitive to water content. Consequently, compared with HFR, R_P^{eff} was more strongly dependent on the operating current density and the RH condition owing to the water content. In addition, R_P^{eff} was less than HFR because of the lower material thickness and change in the mean distance of ionic transport. To identify the effect of the movement differential, H_2/Heliox experiments were conducted. As a consequence, the R_P^{eff} and R_{mass} were varied owing to the diffusion effect. The R_P^{eff} was changed in the H_2/Heliox experiment, especially at high current densities, because the diffusion coefficient was low under H_2/air.

The relationship $R_P^{eff} \approx R_p/3$ was additionally derived from the general solution, but this approximation entailed a relatively large error of more than 5.8% at RH 80% and 7.1% at RH 100% in this experimental condition.

The separation of resistances is helpful in the diagnosis of PEM fuel cells, and the calculation of overpotential is useful in identifying the effect of resistance in terms of voltage.

Author Contributions: Conceptualization and Methodology, J.C. and K.M.; Investigation, J.C. and J.S.; Analysis, J.C., J.S., H.O., and K.M.; Writing, J.C., J.S., H.O., and K.M.; Supervision, K.M. All authors have read and agreed to the published version of the manuscript.

Funding: This research received no external funding.

Acknowledgments: This work was granted financial resources from the SNU Institute of Advanced Machines and Design (IAMD).

Conflicts of Interest: The authors declare no conflict of interest.

Abbreviations

r_p	distributed protonic resistance in the CCL, Ω cm
r_{ct}	distributed charge transfer resistance, Ω cm
z_W	distributed BCPE, Ω cm
r_{mass}	distributed mass transport resistance, Ω cm
q_C	parameter related to CPE, Ω^{-1} cm^{-3} s^{P_c}
P_C	CPE exponent
q_B	distributed parameter related to BCPE, Ω^{-1} cm^{-3} s^{P_B}
P_B	BCPE exponent
k	iteration number of the node, $1 \leq k \leq n-1$
n	total repeating number of the node
HFR	high frequency resistance, Ω cm^2
R_p	protonic resistance in the CCL, Ω cm^2
R_p^{eff}	effective protonic resistance in the CCL, Ω cm^2
R_{ct}	charge transfer resistance, Ω cm^2
Z_W	BCPE, Ω cm^2
R_{mass}	mass transfer resistance, Ω cm^2
R_{ohmic}	ohmic resistance, Ω cm^2
R_{total}	total resistance, Ω cm^2
Q_C	parameter related to CPE, Ω^{-1} cm^{-2} s^{P_c}
Q_B	parameter related to BCPE, Ω^{-1} cm^{-2} s^{P_B}
D^{eff}	effective diffusion coefficient of oxygen diffusion in the CCL, cm^2 s^{-1}
x	non-dimensional distance along the catalyst layer, $0 \leq x \leq 1$
l	thickness of the CCL, cm
σ	proton conductivity, $\sigma = \sigma_{el}/l$, S cm^{-2}
σ_{el}	specific proton conductivity, S cm^{-1}
m_{mass}	mass transport coefficient, V
n_{mass}	simulation parameter for the polarization curve fitting, cm^2 A^{-1}
b	Tafel slope, V
E	cell voltage, V
E_0	open-circuit voltage (OCV), V
j	current density distribution along the CCL, A cm^{-2}
i^*	exchange current density, A cm^{-2}
I	current density, A cm^{-2}
η_1	overpotential at the PEM/CCL interface, V
i	imaginary component in impedance
w	frequency, Hz
F	Faradaic constant, 96,487 A s mol^{-1}
P	total pressure, Pa
T	temperature, K
R	Gas constant, 8.314 J K^{-1} mol^{-1}

Subscripts	
C	constant phase element (CPE)
B	bounded constant phase element (BCPE)
ct	Charge transfer
$ohmic$	ohmic
$mass$	mass transport
k	iteration number of the node, $1 \leq k \leq n-1$
n	total repeating number of the node

References

1. Cruz-Manzo, S.; Chen, R. A generic electrical circuit for performance analysis of the fuel cell cathode catalyst layer through electrochemical impedance spectroscopy. *J. Electroanal. Chem.* **2013**, *694*, 45–55. [CrossRef]
2. Park, J.; Oh, H.; Ha, T.; Lee, Y.I.; Min, K. A review of the gas diffusion layer in proton exchange membrane fuel cells: Durability and degradation. *Appl. Energy* **2015**, *155*, 866–880. [CrossRef]
3. Wang, Y.; Chen, K.S.; Mishler, J.; Cho, S.C.; Adroher, X.C. A review of polymer electrolyte membrane fuel cells: Technology, applications, and needs on fundamental research. *Appl. Energy* **2011**, *88*, 981–1007. [CrossRef]
4. Brunetto, C.; Moschetto, A.; Tina, G. PEM fuel cell testing by electrochemical impedance spectroscopy. *Electr. Power Syst. Res.* **2009**, *79*, 17–26. [CrossRef]
5. Page, S.C.; Anbuky, A.H.; Krumdieck, S.P.; Brouwer, J. Test Method and Equivalent Circuit Modeling of a PEM Fuel Cell in a Passive State. *IEEE Trans. Energy Convers.* **2007**, *22*, 764–773. [CrossRef]
6. Wu, J.; Yuan, X.Z.; Wang, H.; Blanco, M.; Martin, J.J.; Zhang, J. Diagnostic tools in PEM fuel cell research: Part I Electrochemical techniques. *Int. J. Hydrogen Energy* **2008**, *33*, 1735–1746. [CrossRef]
7. Kulikovsky, A. A physical model for catalyst layer impedance. *J. Electroanal. Chem.* **2012**, *669*, 28–34. [CrossRef]
8. Malevich, D.; Halliop, E.; Peppley, B.A.; Pharoah, J.G.; Karan, K. Investigation of Charge-Transfer and Mass-Transport Resistances in PEMFCs with Microporous Layer Using Electrochemical Impedance Spectroscopy. *J. Electrochem. Soc.* **2009**, *156*, B216–B224. [CrossRef]
9. Van der Merwe, J.; Uren, K.; van Schoor, G.; Bessarabov, D. Characterisation tools development for PEM electrolysers. *Int. J. Hydrog. Energy* **2014**, *39*, 14212–14221. [CrossRef]
10. Yoo, H.D.; Jang, J.H.; Ka, B.H.; Rhee, C.K.; Oh, S.M. Impedance Analysis for Hydrogen Adsorption Pseudocapacitance and Electrochemically Active Surface Area of Pt Electrode. *Langmuir* **2009**, *25*, 11947–11954. [CrossRef]
11. Lefebvre, M.C.; Martin, R.B.; Pickup, P.G. Characterization of Ionic Conductivity Profiles within Proton Exchange Membrane Fuel Cell Gas Diffusion Electrodes by Impedance Spectroscopy. *Electrochem. Solid-State Lett.* **1999**, *2*, 259–261. [CrossRef]
12. Eikerling, M.; Kornyshev, A. Electrochemical impedance of the cathode catalyst layer in polymer electrolyte fuel cells. *J. Electroanal. Chem.* **1999**, *475*, 107–123. [CrossRef]
13. Makharia, R.; Mathias, M.F.; Baker, D.R. Measurement of Catalyst Layer Electrolyte Resistance in PEFCs Using Electrochemical Impedance Spectroscopy. *J. Electrochem. Soc.* **2005**, *152*, A970–A977. [CrossRef]
14. Freire, T.J.; Gonzalez, E.R. Effect of membrane characteristics and humidification conditions on the impedance response of polymer electrolyte fuel cells. *J. Electroanal. Chem.* **2001**, *503*, 57–68. [CrossRef]
15. Vielstich, W.; Gasteiger, H.A.; Lamm, A.; Yokokawa, H. *Handbook of Fuel Cells, Fundamentals, Technology and Applications*; John Wiley & Sons, Ltd.: Hoboken, NJ, USA, 2010.
16. Gaumont, T.; Maranzana, G.; Lottin, O.; Dillet, J.; Guétaz, L.; Pauchet, J. In Operando and Local Estimation of the Effective Humidity of PEMFC Electrodes and Membranes. *J. Electrochem. Soc.* **2017**, *164*, F1535–F1542. [CrossRef]
17. Neyerlin, K.C.; Gu, W.; Jorne, J.; Clark, A.; Gasteiger, H.A. Cathode catalyst utilizationfor the ORR in a PEMFC—Analytical model and experimental validation. *J. Electrochem. Soc.* **2007**, *154*, B279–B287. [CrossRef]
18. Liu, Y.; Murphy, M.W.; Baker, D.R.; Gu, W.; Ji, C.; Jorne, J.; Gasteiger, H.A. Proton Conduction and Oxygen Reduction Kinetics in PEM Fuel Cell Cathodes: Effects of Ionomer-to-Carbon Ratio and Relative Humidity. *J. Electrochem. Soc.* **2009**, *156*, B970–B980. [CrossRef]
19. Lange, K.J.; Sui, P.-C.; Djilali, N. Pore scale modeling of a proton exchange membrane fuel cell catalyst layer: Effects of water vapor and temperature. *J. Power Sources* **2011**, *196*, 3195–31203. [CrossRef]
20. Kim, J.-R.; Yi, J.S.; Song, T.-W. Investigation of degradation mechanisms of a high-temperature polymer-electrolyte-membrane fuel cell stack by electrochemical impedance spectroscopy. *J. Power Sources* **2012**, *220*, 54–64. [CrossRef]
21. Kulikovsky, A.A. Can We Quantify Oxygen Transport in the Nafion Film Covering an Agglomerate of Pt/C Particles? *J. Electrochem. Soc.* **2017**, *164*, F379–F386. [CrossRef]
22. Jaouen, F.; Lindbergh, G. Transient Techniques for Investigating Mass-Transport Limitations in Gas Diffusion Electrodes I. Modeling the PEFC Cathode. *J. Electrochem. Soc.* **2003**, *150*, A1699–A16710. [CrossRef]
23. Malevich, D.; Pharoah, J.; Peppley, B.; Karan, K. On the Determination of PEM Fuel Cell Catalyst Layer Resistance from Impedance Measurement in H2/N2 Cells. *ECS Meet. Abstr.* **2011**, *159*, F888–F895. [CrossRef]
24. Gerteisen, D. Impact of Inhomogeneous Catalyst Layer Properties on Impedance Spectra of Polymer Electrolyte Membrane Fuel Cells. *J. Electrochem. Soc.* **2015**, *162*, F1431–F1438. [CrossRef]

25. Cruz-Manzo, S.; Chen, R.; Greenwood, P. An impedance model for analysis of EIS of polymer electrolyte fuel cells under hydrogen peroxide formation in the cathode. *J. Electroanal. Chem.* **2015**, *745*, 28–36. [CrossRef]
26. Cooper, K.; Smith, M. Electrical test methods for on-line fuel cell ohmic resistance measurement. *J. Power Sources* **2006**, *160*, 1088–1095. [CrossRef]
27. Guo, Q.; White, R.E. A Steady-State Impedance Model for a PEMFC Cathode. *J. Electrochem. Soc.* **2004**, *151*, E133–E149. [CrossRef]
28. Tang, Y.; Zhang, J.; Song, C.; Liu, H.; Zhang, J.; Wang, H.; MacKinnon, S.; Peckham, T.; Li, J.; McDermid, S.; et al. Temperature Dependent Performance and In Situ AC Impedance of High-Temperature PEM Fuel Cells Using the Nafion-112 Membrane. *J. Electrochem. Soc.* **2006**, *153*, A2036–A2043. [CrossRef]
29. Eikerling, M.; Kornyshev, A. Modelling the performance of the cathode catalyst layer of polymer electrolyte fuel cells. *J. Electroanal. Chem.* **1998**, *453*, 89–106. [CrossRef]
30. Yuan, X.; Wang, H.; Sun, J.C.; Zhang, J. AC impedance technique in PEM fuel cell diagnosis—A review. *Int. J. Hydrogen Energy* **2007**, *32*, 4365–4380. [CrossRef]
31. Rezaei Niya, S.M.; Hoorfar, M. Study of proton exchange membrane fuel cells using electrochemical impedance spectroscopy technique—A review. *J. Power Sources* **2013**, *240*, 281–293. [CrossRef]
32. Asghari, S.; Mokmeli, A.; Samavati, M. Study of PEM fuel cell performance by electrochemical impedance spectroscopy. *Int. J. Hydrogen Energy* **2010**, *35*, 9283–9290. [CrossRef]
33. Springer, T.E.; Raistrick, I.D. Electrical Impedance of a Pore Wall for the Flooded-Agglomerate Model of Porous Gas-Diffusion Electrodes. *J. Electrochem. Soc.* **1989**, *136*, 1594–1603. [CrossRef]
34. Wagner, N. Characterization of membrane electrode assemblies in polymer electrolyte fuel cells using a.c. impedance spectroscopy. *J. Appl. Electrochem.* **2002**, *32*, 859–863. [CrossRef]
35. Kim, J.; Lee, S.; Srinivasan, S.; Chamberlin, C.E. Modeling of Proton Exchange Membrane Fuel Cell Performance with an Empirical Equation. *J. Electrochem. Soc.* **1995**, *142*, 2670–2674. [CrossRef]
36. Xu, H.; Song, Y.; Knuz, H.R.; Fenton, J.M. Effect of Elevated Temperature and Reduced Relative Humidity on ORR Kinetics for PEM Fuel Cells. *J. Electrochem. Soc.* **2005**, *152*, A1828–A1836. [CrossRef]
37. Jaouen, F.; Lindbergh, G.; Wiezell, K. Transient Techniques for Investigating Mass-Transport Limitations in Gas Diffusion Electrodes II. Experimental Characterization of the PEFC Cathode. *J. Electrochem. Soc.* **2003**, *150*, A1711–A1717. [CrossRef]
38. Dotelli, G.; Omati, L.; Stampino, P.G.; Brivio, D.; Grassini, P. Effect of Micro Porous Layer (MPL) on Water Management Investigated by Electrochemical Impedance Spectroscopy (EIS) on a Running PEM-FC. *ECS Trans.* **2010**, *33*, 1115–1122. [CrossRef]
39. Zhang, J.; Tang, Y.; Song, C.; Xia, Z.; Li, H.; Wang, H.; Zhang, J. PEM fuel cell relative humidity (RH) and its effect on performance at high temperatures. *Electrochim. Acta* **2008**, *53*, 5315–5321. [CrossRef]
40. Cappadonia, M.; Erning, J.; Niaki, S.M.; Stimming, U. Conductance of Nafion 117 membranes as a function of temperature and water content. *Solid State Ionics* **1995**, *77*, 65–69. [CrossRef]
41. Uosaki, K.; Okazaki, K.; Kita, H. Conductivity of Nation membranes at low temperatures. *J. Electroanal. Chem. Interfacial Electrochem.* **1990**, *287*, 163–169. [CrossRef]